Infrared Physics & Technology 131 (2023) 104662

Contents lists available at ScienceDirect

Infrared Physics and Technology

journal homepage: www.elsevier.com/locate/infrared

The optical properties of In_2S_3 films in the far-infrared spectral range

Bohdan Andriyevsky [a,*], Leszek Bychto [a], Krzysztof Dorywalski [b], Ulrich Schade [c], Ljiljana Puskar [c], Aleksy Patryn [a], Aneta Hapka [a], Katarzyna Mydłowska [d], Alexander Veber [c,e], Andrii I. Kashuba [f], K.T. Ramakrishna Reddy [g]

[a] Faculty of Electronics and Computer Sciences, Koszalin University of Technology, Śniadeckich str. 2, PL-75-453, Koszalin, Poland
[b] Institute of Experimental Physics, Faculty of Mathematics, Physics and Informatics, University of Gdańsk, Wita Stwosza 57, 80-308 Gdańsk, Poland
[c] Institute for Electronic Structure Dynamics, Helmholtz-Zentrum Berlin für Materialien und Energie GmbH, Albert-Einstein-Strasse 15, 12489 Berlin, Germany
[d] Faculty of Mechanical Engineering, Koszalin University of Technology, Śniadeckich str. 2, PL-75-453, Koszalin, Poland
[e] Department of Chemistry, Humboldt Universität zu Berlin, Brook-Taylor-Straße 2, 12489 Berlin, Germany
[f] Department of General Physics, Lviv Polytechnic National University, Bandera str. 12, 79013 Lviv, Ukraine
[g] Sri Venkateswara University, Tirupati, 517 502, Andhra Pradesh, India

ARTICLE INFO

Keywords:
Semiconductors
In_2S_3 thin films
Free electrons
Localized electrons
Optical conductivity
Phonon spectra

ABSTRACT

Optical reflection spectra of In_2S_3 thin films (180 – 730 nm) deposited on glass substrates are measured by infrared spectroscopy using the synchrotron radiation of BESSY II storage ring in the spectral range of 30 – 8000 cm^{-1}. The aim of the study is to find the influence of different substrate and post-annealing temperatures on the electron and phonon systems of In_2S_3 films deposited on glass. Clear features in the reflectance spectra for the studied films have been found mainly in the phonon excitation range 100 – 400 cm^{-1}. The experimental dielectric functions $\varepsilon(\omega)$ of In_2S_3 films are found to be in good agreement with the calculated ones obtained for In_2S_3 crystals within the density functional theory. The dielectric functions $\varepsilon(\omega)$ of the films in the range of 100 – 400 cm^{-1} depend substantially on the post-annealing temperature. This indicates a transition of the film from the amorphous to the crystalline state. The thorough analysis of the frequency dependence of the reflection coefficient $R(\omega)$ and optical conductivity $\sigma(\omega)$ in the wavenumber range of 30 – 130 cm^{-1} allowed us to reveal the distributed electron states in In_2S_3 films.

1. Introduction

Indium sulfide (In_2S_3) semiconductor is used as a buffer layer in the photovoltaic thin-film solar cells based on Cu(In, Ga)Se_2 (CIGS) [1,2]. CIGSis known to be a material for solar cells with excellent properties, such as high absorption coefficient, tunable bandgap, and satisfactory environmental qualities [3–5]. On a laboratory scale, Cu (In, Ga)$(S, Se)_2$ thin-film cells achieved the power conversion efficiency of about 23 % [6]. The structure of this efficient CIGS solar cell comprises of Glass/Mo/CIGS/Buffer layer/i-ZnO/*n*-ZnO:Al. It incorporates cadmium sulfide (CdS) as a buffer layer between the CIGS main absorber and window layers. However, because of the cadmium toxicity, CdS is not a best choice as a buffer in solar cells [7,8]. Furthermore, the bandgap of CdS ($E_g = 2.4$ eV) is not sufficiently large for the short-wavelength photons of the daylight to reach the CIGS main absorption layer [7,8]. Hence, replacing CdS buffer layer with other Cd-free materials has attracted considerable attention and is considered as one of the main goals in the field of CIGS thin film solar cells [7,8]. From this viewpoint, In_2S_3, which can have the bandgap larger than $E_g = 2.4$ eV is an interesting alternative. Using an In_2S_3 buffer layer in Cu(In, Ga)Se_2 the relatively high photocurrent conversion efficiency of 18.2 % was reported [9], which is close to the value achieved using CdS buffer layer. It is important to emphasize that the electronic and consequently optical properties of In_2S_3 films depend substantially on the stoichiometry and preparation conditions of the deposited layers.

One of the main material characteristics important for the above mentioned application is the charge carrier (electrons) concentration (N_c) of the deposited films and its relation to other optical and electronic

* Corresponding author.
E-mail addresses: bohdan.andriyevskyy@tu.koszalin.pl (B. Andriyevsky), leszek.bychto@tu.koszalin.pl (L. Bychto), krzysztof.dorywalski@ug.edu.pl (K. Dorywalski), ulrich.schade@helmholtz-berlin.de (U. Schade), ljiljana.puskar@helmholtz-berlin.de (L. Puskar), aleksy.patryn@tu.koszalin.pl (A. Patryn), aneta.hapka@tu.koszalin.pl (A. Hapka), katarzyna.mydlowska@tu.koszalin.pl (K. Mydłowska), alexander.veber@helmholtz-berlin.de (A. Veber), andrii.i.kashuba@lpnu.ua (A.I. Kashuba), ktrkreddy@svuniversity.ac.in (K.T.R. Reddy).

https://doi.org/10.1016/j.infrared.2023.104662
Received 3 February 2023; Received in revised form 14 March 2023; Accepted 21 March 2023
Available online 24 March 2023

properties. This problem remains important for In_2S_3 films [10 –12]. The charge carrier concentration of the films prepared at different conditions can be estimated from the reflectance spectra of the material. Depending on the magnitude of the free electron concentration N_c in the samples, the spectral features corresponding to the plasma reflection are expected to appear at different parts of the spectrum. This may be evaluated by using the known relation of the Drude-Lorentz model of conductivity between the plasma frequency ω_p and charge carrier concentration N_c,

$$\omega_p^2 = \frac{N_c e^2}{\varepsilon_0 \varepsilon_\infty m^*} \ , \ (in\ rad/s) \tag{1}$$

where e is the electron charge, $\varepsilon_0 = 8.85{\cdot}10^{-12}$F/m is the dielectric constant of vacuum, m^* is the effective mass of the charge carriers (electrons or holes) in a material [13]. The Table 1 presents the numerical correspondence between the plasma frequency ω_p and the electron concentration N_c, according to the relation (1), when the effective mass m^* is equal to the free electron mass, $m^* = m_e$.

The relation (1) may be used to calculate the electron concentration, N_c in In_2S_3 films by the determination of plasma frequency ω_p from the measured reflectance spectrum [14,15].

Apart from the spectral features caused by the electron plasma excitations in the extrinsic semiconductors, the phonon related features of the materials are also present in the mid- and far-IR spectral range. Dielectric functions obtained in this range may deliver information on the features of interatomic bonding of the studied In_2S_3 films obtained at different deposition and post-annealing temperatures.

The additional *ab initio* calculations based on the density functional theory (DFT) of the electron and phonon properties of In_2S_3 crystals are performed in the present study to derive more valid conclusions on this material.

2. Methods of investigation

2.1. Experimental methods

The In_2S_3 films were deposited by thermal evaporation technique using In_2S_3 powder as a source material. The films were deposited on soda-lime glass substrates at a constant temperature (T_s) of 200, 250, 300, and 350 °C by maintaining a source to substrate distance of 14 cm and deposition rate of 15 Å/*sec*. The thickness of the films, measured by the piezo-electric method using the quartz crystal thickness monitor, were found to be in the range of 69 – 656 nm (Table 2). The as-grown films were annealed in vacuum ($2{\cdot}10^{-2}$ mbar) at various temperatures (T_a) in the range of 200–300 °C for 60 min [10].The films are of relatively good optical quality, they are semitransparent, and without substantial visible light scattering.

The structural analysis of In_2S_3 films was carried out by means of X-ray diffraction in grazing incidence diffraction geometry (GIXRD), using Empyrean diffractometer (Malvern Panalytical, UK) with Cu-Kα radiation source (λ = 1.5406 Å). The incidence angle was set to 1°, which ensured the radiation penetration depth of max. 400 nm. The analysis of the results was carried out with the use of HighScore Plus software combined with the database of diffraction patterns ICDD PDF 4 + 2022.

Measurements of the specular reflectance of In_2S_3 films were performed at an angle of incidence angle of 9° using the synchrotron radiation of BESSY II storage ring at the IRIS beamline of HZB (Berlin). The high brilliance of the synchrotron radiation together with a Fourier-transform infrared (FTIR) Bruker Vertex 70/v spectrometer allow for a precise measurement of reflectance spectra of the samples by applying a quasi-normal incidence set-up as further described in [16] with a gold film as reference. Measurements could be performed with undefined polarization of the radiation due to the un-isotropy of the samples. The samples have been placed in a cryostat for measurement at ambient temperature and at 5 K close to the liquid helium temperature. Spectra have been recorded with a mechanically cooled transition edge superconducting bolometer (QMC) in the spectral range between 20 and 500 cm^{-1} with the resolution of 4 cm^{-1}. FIR detector used was Cryogen free THz bolometer made by QMC instruments. It is a closed cycle Niobium transition edge sensor (TES) superconducting bolometer.

Table 2
Thicknesses (in nm) of In_2S_3 films on glass substrates prepared at different substrate (T_{si}) and post-annealing (T_{aj}) temperatures.

T_{si} /°C T_{aj} /°C	200 °C ($i = 1$)	250 °C ($i = 2$)	300 °C ($i = 3$)	350 °C ($i = 4$)
20 °C ($j = 1$)	182	575	510	264
200 °C ($j = 2$)	430	69	504	253
250 °C ($j = 3$)	239	591	384	293
300 °C ($j = 4$)	152	656		232

The measured reflectance spectra $R(\omega)$ were used to calculate the complex dielectric function $\varepsilon = \varepsilon_1 + i\varepsilon_2$ (and derived values of the refractive indices, electrical conductivity, and others) using Kramers-Kronig transformation and the RefFIT software [17]. The following Drude-Lorentz model for the dielectric function $\varepsilon = \varepsilon_1 + i\varepsilon_2$ is used for fitting the experimental reflectance spectra,

$$\varepsilon(\omega) = \varepsilon_\infty + \sum_i \frac{\omega_{pi}^2}{\omega_{0i}^2 - \omega^2 - i\gamma_i\omega} \tag{2}$$

It describes the optical response of a set of harmonic (damped) oscillators, where ε_∞ is the 'high-frequency dielectric permittivity', which represents contribution from the electron oscillators of the bonded electrons to the total dielectric function ε(ω) of a material. The parameters ω_{pi}, ω_{0i} and γ_i are the 'plasma' frequency, the natural frequency (eigen-frequency) and the line-width (damping rate), respectively, for the Drude free electrons term and Lorentz phonon oscillators. For the Drude free electrons term the corresponding natural frequency, ω_{0i} is equal to zero [17].

2.2. Theoretical method

The theoretical electron and phonon properties of In_2S_3 crystals were calculated in the framework of the density functional theory using the VASP code [18 –23]with the projector augmented wave (PAW_PBE) pseudopotentials [23]. The revised Perdew-Burke-Ernzerhof exchange-and-correlation functional for solids (PBEsol) based on the generalized gradient approximation (GGA) [24] has been utilized.

The crystal structure of the tetragonal β-In_2S_3phase ($I4_1/amd$, no. 141), corresponding to room temperature, was taken for calculations of the phonon spectra using the density-functional-perturbation theory (DFPT) approach. The other two crystal phases of In_2S_3, α ($Fd\ \overline{3}\ m$, no.

Table 1
Plasma frequency ω_p (in different units) calculated using the Drude-Lorentz model (1) for different free electron concentrations N_c, when the effective mass m^* is equal to the free electron mass, $m^* = m_e$, and $\varepsilon_\infty = 1$.

N_c /cm^{-3}	$1{\cdot}10^{14}$	$1{\cdot}10^{15}$	$1{\cdot}10^{16}$	$1{\cdot}10^{17}$	$1{\cdot}10^{18}$	$1{\cdot}10^{19}$	$1{\cdot}10^{20}$
ω_p /cm^{-1}	2.99	9.46	29.9	94.6	299	946	2993
ω_p /rad·s^{-1}	$5.64{\cdot}10^{11}$	$1.78{\cdot}10^{12}$	$5.64{\cdot}10^{12}$	$1.78{\cdot}10^{13}$	$5.64{\cdot}10^{13}$	$1.78{\cdot}10^{14}$	$5.64{\cdot}10^{14}$
ω_p /Hz	$8.98{\cdot}10^{10}$	$2.84{\cdot}10^{11}$	$8.98{\cdot}10^{11}$	$2.84{\cdot}10^{12}$	$8.98{\cdot}10^{12}$	$2.84{\cdot}10^{13}$	$8.98{\cdot}10^{13}$
ω_p /eV	$3.71{\cdot}10^{-4}$	$1.17{\cdot}10^{-3}$	$3.71{\cdot}10^{-3}$	$1.17{\cdot}10^{-2}$	$3.71{\cdot}10^{-2}$	0.117	0.371
ω_p /K	4.3	13.6	43.0	136	430	1362	4306

227) and γ($P\bar{3}m1$, no. 164), relate to higher temperatures (749 K and 1099 K, correspondingly) [25].The electrons 5 s^2 and $5p^1$ for In and 3 s^2 and $3p^4$ for S were treated as valence ones. The plane wave energy cut-off, 520 eV was used for calculations. Monkhorst pack grid 5 × 5 × 1 for the supercell of the dimensions $a = b = 7.6724$ Å, $c = 32.6870$ Å was chosen. All the structures were fully relaxed with an energy convergence of 10^{-8} eV. Hellman–Feynman force per atom was minimized to<0.001 eV/Å.

The dielectric permittivities, ε_∞ (dielectric permittivity caused by the bonding electrons) and ε_{stat} (static dielectric permittivity), were calculated by VASP (PAW_PBE pseudopotentials, xc-functional PBEsol, cut-off energy 520 eV) and CASTEP (norm-conserving pseudopotentials, PBE exchange-and-correlation functional, cut-off energy 800 eV) codes [26].

The effective electron mass m^* of In_2S_3 was calculated using the AMSET code [27] developed on the basis of VASP and BoltzTraP2 codes [18 –23,28]. Before calculations of the electron effective mass using AMSET code, the DFT calculations of the electronic band structure were performed using VASP. Apart from the calculation of the effective electron mass m^*, the calculations of the electron/hole electric conductivity σ and the electron/hole scattering rate $\gamma = \tau^{-1}$ are realized by using the AMSET code. In the AMSET code, different models of the electron/hole scattering are implemented (e.g. acoustic deformation potential, polar optical phonon scattering, and ionized impurity), allowing us to obtain the reliable values of the carrier relaxation time τ in the material studied. Before calculations of the electric conductivity σ and the electron/hole scattering rate γ of the crystal studied by the AMSET code, the VASP code was used to calculate the corresponding elastic constants, the dielectric permittivity ε_∞ caused by the bonding electrons, and the static dielectric permittivity ε_{stat} (electron and phonon parts).

3. Results and discussion

3.1. XRD analysis of In_2S_3 films

The lack of clear diffraction peaks on the diffraction pattern of the as-deposited film indicates its amorphous structure. Annealing the film at 200 °C does not initiate crystallization and the film remains amorphous. Films annealed at 250 °C and 300 °C showed well defined peaks and had polycrystalline structure. Based on matching of the diffraction patterns, it was found that all the observed XRD peaks originate from a single crystalline phase, namely β-In_2S_3, typical for this type of films. The preferred (311) plane orientation is observed for both films. The intensity of the dominant peak and its relation to other peak intensities for the film annealed at 300 °C slightly decreases. A clear rise of the background above 2θ = 15° (wide amorphous halo) can also be observed when the film is heated to higher temperatures, which confirms the presence of an amorphous phase in the film with a slightly lower crystallinity (Fig. 1).

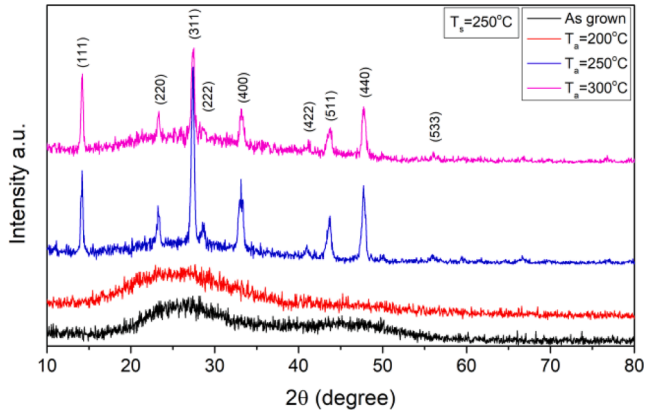

Fig. 1. X-ray diffractograms of In_2S_3 films deposited on the glass substrates at the temperature T_s = 250 °C for different post-annealing temperatures T_a.

Table 3 summarizes the structural parameters of the films annealed at 250 and 300 °C, determined from the observed diffraction patterns. The interplanar lattice spacing was calculated on the basis of Bragg's law according to the formula,

$$d = \frac{n\lambda}{2sin\theta} \quad (3)$$

where: $n = 1$, λ is X-ray wavelength, and θ is Bragg's angle. The size of crystallites in the coating was estimated from the width of the diffraction peaks using the Debye-Sherrer equation,

$$D = \frac{K\lambda}{\beta cos\theta} \quad (4)$$

where $K = 0.94$ (shape dependent factor), and β is full width at half maximum (FWHM) of dominant peak. The lattice strain in the films was calculated by using the relation,

$$\varepsilon = \frac{\beta}{4\tan\theta} \quad (5)$$

The calculations based on the parameters of the dominant peak showed that the crystallographic parameters of the films annealed at both temperatures are close to each other. With an increase of annealing temperature, the interplanar spacing and lattice deformation slightly decrease and there is a slight increase of crystallite size.

3.2. Optical properties of In_2S_3 films

In the present study, the reflection spectra of In_2S_3 films are presented only in the spectral range of 30 – 400 cm^{-1}, where the phonon and electron plasma excitations of the films were detected. For In_2S_3 films studied, no clear reflection spectra features were found in the spectral range of 400 – 8000 cm^{-1}, where the excitations of the localized electronic donor states in In_2S_3 films might in principle take place [10 –12].

The reflectance spectra of In_2S_3 films obtained in the far-infrared range (Fig. 2) contain the clear phonon caused reflection spectral bands in the range of 150 – 340 cm^{-1} and a monotonous decrease of the reflection coefficient $R(\omega)$ in the range of 30 – 150 cm^{-1}. Similar structure of the reflectance spectrum was observed for the layered crystals of $In_2S_{3-x}Se_x$ for $2.4 \leq x \leq 3.0$ [29]. The phonon structure of the reflection spectra $R(\omega)$ of the studied In_2S_3 thin films in the range 150 – 340 cm^{-1} (Fig. 2) will be discussed in the second part of this subchapter.

Due to the small thickness of the films studied in this work the substrate influences the observed IR reflectance spectra, which is in particular visible in the range below 140 cm^{-1}. According to the literature data a soda-lime glass possesses an absorption bands in the far-IR region due to Me-O vibrations [30]. To include the glass contribution in the experimental spectra we have measured separately the glass substrate at the same experimental conditions and referenced the In_2S_3 thin film spectra using the glass spectra obtained and the RefFIT software. The obtained fitting parameters of In_2S_3 films were used for the further analysis.

According to the Maxwell's equations, the complex dielectric function $\varepsilon = \varepsilon_1 + i\varepsilon_2$ and the complex optical conductivity $\sigma = \sigma_1 + i\sigma_2$, of a material are related to each other as [31],

Table 3
Parameters of XRD patterns of In_2S_3 films deposited at the temperature T_s = 250 °C for two post-annealing temperatures, T_a = 250 °C and T_a = 300 °C.

T_a /°C	2θ /°	β /rad	d/Å	D/nm	$\varepsilon \cdot 10^{-3}$
250	27.397	0.0068	3.253	21.9	7.0
300	27.423	0.0065	3.250	22.9	6.6

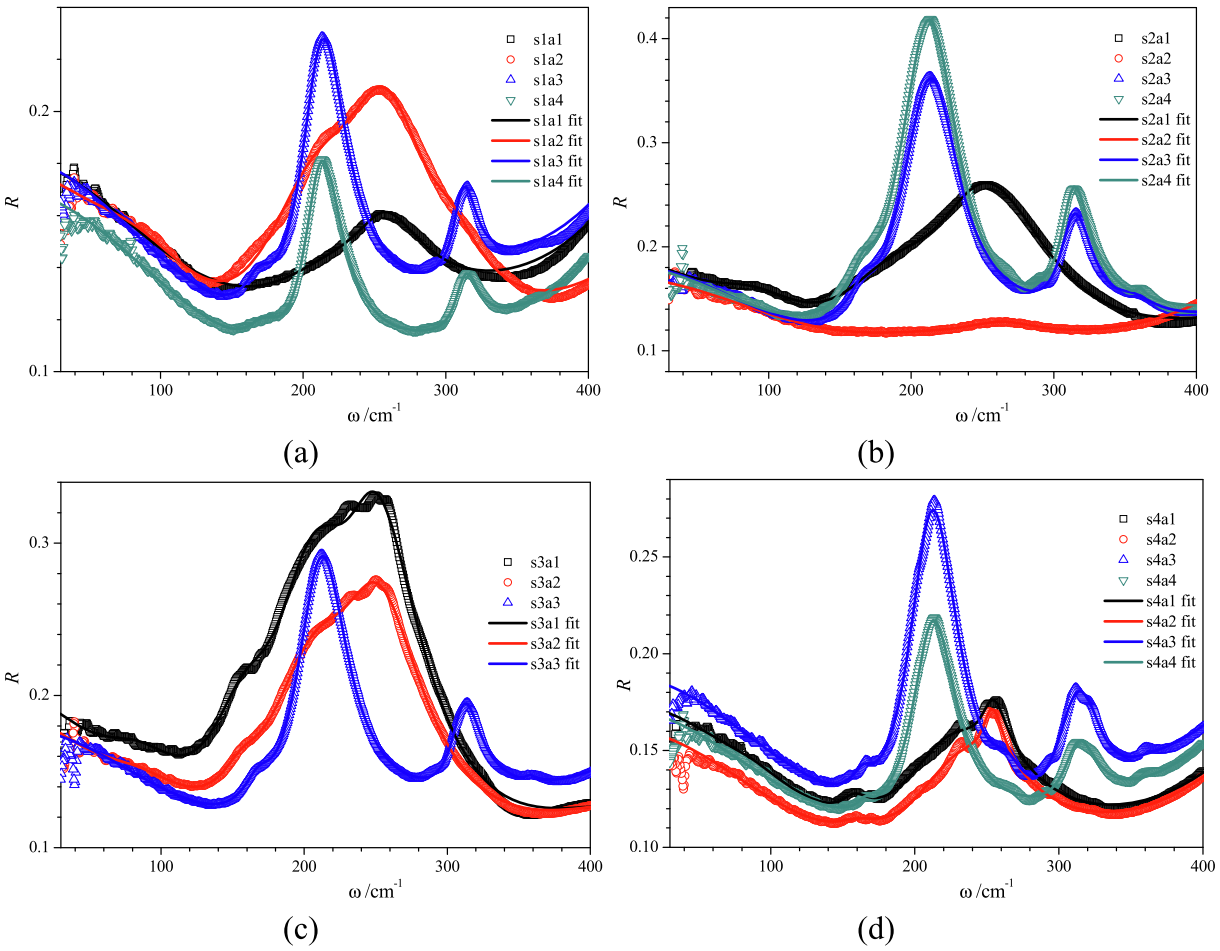

Fig. 2. Experimental reflectance spectra $R(\omega)$ of In_2S_3 films obtained at different substrate temperatures, $T_{s1} = 200$ °C, $T_{s2} = 250$ °C, $T_{s3} = 300$ °C, $T_{s4} = 350$ °C, and post-annealing temperaures, $T_{a1} = 20$ °C, $T_{a2} = 200$ °C, $T_{a3} = 250$ °C, $T_{a4} = 300$ °C (see Table 2). Solid lines represent results of fitting. The four abbreviation symbols of curves are composed of two sub-symbols of substrate temperatures and two sub-symbols of the annealing temperatures.

$$\varepsilon = \frac{i\sigma}{\varepsilon_0 \omega} \tag{6}$$

As a result, the real part of conductivity σ_1 is directly proportional to the imaginary part of dielectric function ε_2,

$$\sigma_1 = \varepsilon_0 \varepsilon_2 \omega \tag{7}$$

Thus, by measuring the reflective spectra of materials $R(\omega)$ one can calculate the dielectric function $\varepsilon(\omega)$ by using the Kramers-Kronig relation and, afterward, the optical conductivity σ_1, which is necessary in order to estimate the corresponding carrier density N_c, relaxation time τ, and effective electron/hole masses m^*.

According to the Drude-Lorentz approach [15,17] and estimated plasma frequency (Table 1) the decreasing dependence of $R(\omega)$ in the spectral range of 30 – 150 cm^{-1} (Fig. 2) can be caused, apart from the mentioned above spectral features of the soda-lime glass substrate, also by the interaction of free electrons with the far-IR radiation. This interaction corresponds to the intra-band optical transitions with the transverse frequency $\omega_{0i} = \omega_{01} = 0$ in the relation (2). The obtained fitting parameter γ in the RefFIT software represents the carrier relaxation time, $\tau = 1/\gamma$, whereas the obtained plasma frequency, ω_p, can be used for calculation of the quotient N_c/m^* (1). The latter value can be used to obtain the effective electron mass m^* if the carrier concentration N_c is known. From the fitted experimental reflection spectra $R(\omega)$ of In_2S_3 films the spectra of complex optical conductivity $\sigma(\omega)$ were calculated using RefFIT software. The real part of the electric conductivity at $\omega = 0$, $\sigma_1(\omega = 0) = \sigma_{stat}$, can be used to calculate the electric carrier concentration N_c using the following equation,

$$N_c = \frac{\sigma_{stat}}{e\mu} \tag{8}$$

if the reference value of the electron mobility μ for In_2S_3 is known. However this is not a trivial task, since the exact value of the free electron mobility in In_2S_3 thin films is unknown and different values can be found in the literature, e.g. in Ref. [32] $\mu = 400$ $cm^2V^{-1}s^{-1}$ and in Ref. [33] $\mu \leq 5$ $cm^2V^{-1}s^{-1}$. Therefore, in addition to the literature data, we have calculated the free electron mobility μ, and other related values for β-In_2S_3 crystal (space group of symmetry no. 141) using the DFT codes VASP and AMSET.

The fitting results related to the high-frequency (ε_∞) and static (ε_{stat}) dielectric permittivity of In_2S_3 films are given in Table 4. The static dielectric permittivity ε_{stat} is defined as the real part of the complex dielectric permittivity ε calculated by the relation (2) at the frequency $\omega = 0$, $\varepsilon_{stat} = \mathrm{Re}(\varepsilon)|_{\omega = 0}$. The values averaged over different substrate

Table 4
Dielectric permittivity ε_∞ and ε_{stat} ($\varepsilon_\infty/\varepsilon_{sta}$) of In_2S_3 films derived from the fitting experimental dependences $R(\omega)$ of In_2S_3 films at different substrate (T_{si}) and annealing (T_{aj}) temperatures.

T_{si} (°C) T_{aj} (°C)	200 °C ($i = 1$)	250 °C ($i = 2$)	300 °C ($i = 3$)	350 °C ($i = 4$)
20 °C ($j = 1$)	7/12.55	6.91/11.43	9.6/16.13	5.7/12.2
200 °C ($j = 2$)	6.51/9.7	8.45/14.69	7.93/12.93	5.32/9.64
250 °C ($j = 3$)	5.67/11.39	6.06/10.46	5.56/11.68	5.28/15.7
300 °C ($j = 4$)	5.56/9.84	6.06/10.87	–	5.48/14.53

temperatures T_s are presented also in Table 5. The averaging over T_s temperature was done to see better the influence of the annealing temperature T_a on the thin film properties. The averaging by the annealing temperature T_a, not by the sample temperature T_s, was chosen because the temperature T_a is found to influence the structural state of In_2S_3 thin films, amorphous or crystalline, which is seen in Fig. 2. For all cases of the films studied the static dielectric permittivity ε_{stat} is larger than the high-frequency-one ε_∞ (Table 4). This is expected when the free electron concentration N_c in the semiconductor is relatively small. The values of the experimental dielectric permittivity of In_2S_3 films, presented in Table 4 are comparable to the corresponding calculated values for In_2S_3 crystal at the space group of symmetry no. 141, obtained using VASP and CASTEP codes based on DFT (Table 5), if taking into account clear differences in theoretical values of ε_{stat} obtained by using these two codes.

The maximum electron concentration obtained is of the order of $N_c^{(RefFIT)} \sim 1{\cdot}10^{15}$ cm^{-3}, which may correspond to the unintentional doping of In_2S_3 samples (Tables 5 and 6). The free electron electric conductivity usually occurs in In_2S_3 films because of sulfur deficiency in the deposited material. With increasing of the annealing temperature T_a an increasing tendency of the free electron concentration $N_c^{(RefFIT)}$ and a decreasing one of the dielectric permittivity $\varepsilon_\infty^{(RefFIT)}$ of In_2S_3 films are observed. The static dielectric permittivity $\varepsilon_{stat}^{(RefFIT)}$ of In_2S_3 films however shows no clear changes (Table 5). The increase of the free electron concentration $N_c^{(RefFIT)}$ with the annealing temperature is in agreement with the experimental results obtained in Ref. [34] for the same types of In_2S_3 thin films.

Using the relations (1) and (8), the fitted values ω_p^2, ε_∞, σ_1, and the reference value of the free electron mobility $\mu = 400$ cm^{2}V^{-1}s^{-1} [32] we calculated the effective electron mass m^*. The averaged (over different substrate and annealing temperatures) value of the effective electron mass $m^*$of In_2S_3 films is about 0.6 m_e (Table 5).

It is interesting to compare the obtained free electron concentration $N_c^{(RefFIT)}$ with the similar values derived from the experimental results of the direct current conductivity of In_2S_3 [34]. According to the latter reference, the electrical conductivity of In_2S_3 in the temperature range of 300 – 450 °C is of the activation character (the activation energy of conductivity E_a was found in the range of 0.51 – 0.73 eV),

$$\sigma = \sigma_0 \exp\left(-\frac{E_a}{k_B T}\right) \tag{9}$$

The activation character of electrical conductivity means that the corresponding conduction band electrons are released by temperature excitation from the local energy states below the bottom conduction band of In_2S_3.

The reported experimental electrical conductivity of In_2S_3 film deposited on the glass substrate at the temperature of $T_s = 350$ °C and annealed at the temperature of $T_a = 300$ °C is $3{\cdot}10^{-5}$ S/cm [34]. This value is about three orders of magnitude lower than the one obtained in this work from the IR-reflection spectra, $\sigma^{(RefFIT)} = 5{\cdot}10^{-2}$ S/cm.

Table 5
Experimental (FTIR spectroscopy and RefFIT fitting) and theoretical (DFT-calculations by VASP, CASTEP, and AMSET codes) of optical and electron parameters of In_2S_3 thin films. Experimental values are presented for different annealing temperatures T_a of thin films.

T_a /°C	20	200	250	300
$\varepsilon_\infty^{(RefFIT)}$	7.30 ± 1.64	7.05 ± 1.42	5.64 ± 0.32	5.7 ± 0.31
$\varepsilon_{stat}^{(RefFIT)}$	5.7 ± 0.31	11.7 ± 2.5	12.3 ± 2.3	11.7 ± 2.5
$\varepsilon_\infty^{(VASP)}$	7.08			
$\varepsilon_\infty^{(CASTEP)}$	5.90			
$\varepsilon_{stat}^{(VASP)}$	13.5			
$\varepsilon_{stat}^{(CASTEP)}$	11.1			
$N_c^{(RefFIT)}$ /10^{14} cm^{-3}	3.92	2.84	8.41	7.85
$m^{*(RefFIT)}$ /m_e	0.47	0.80	0.60	0.63
$m^{*(AMSET)}$ /m_e	0.28			

Table 6
Electrical carrier concentrations N_c (in units of 10^{14} cm^{-3}) corresponding to the fitted optical conductivity σ_1 obtained on the basis of FTIR reflection spectra $R(\omega)$ of In_2S_3 films at different substrate (T_{si}) and annealing (T_{aj}) temperatures for carrier mobility $\mu = 400$ cm^{2}V^{-1}s^{-1}.

T_{si} (°C) T_{aj} (°C)	200 °C ($i = 1$)	250 °C ($i = 2$)	300 °C ($i = 3$)	350 °C ($i = 4$)
20 °C ($j = 1$)	8.21	1.90	2.40	3.19
200 °C ($j = 2$)	2.91	5.71	1.86	0.88
250 °C ($j = 3$)	6.72	2.44	10.1	14.4
300 °C ($j = 4$)	12.0	3.33	–	8.21

According to our estimations the relatively small concentration $N_c \leq 10^{16}$ cm^{-3} results in low plasma frequency value (see Table 1), i.e. the reflection coefficient should be measured with high quality in the spectral range $\omega < 30$ cm^{-1}, which was beyond the conducted experiment, since requires special operation mode of the synchrotron radiation (low α-mode).

The experimental temperature dependence of the electrical conductivity $\sigma(T)$ of the In_2S_3 film [34] is found to be in the relatively good agreement with the results of our DFT-based calculations of In_2S_3 crystal (space group of symmetry no. 141) using VASP and AMSET codes (Fig. 3). Here, the bandgap of $E_g = 0.85$ eV was used for calculations, which is close to the experimentally obtained activation energies of electrical conductivity $E_a \approx 0.5 - 0.6$ eV [34]. Thus, the activation character of the electric conductivity of the studied In_2S_3 thin films has been confirmed theoretically. Fig. 3 shows that for the free electron concentration $N_c \geq 10^{17}$ cm^{-3} in In_2S_3 the temperature dependence of the electric conductivity $\sigma(T)$ become of the metal-like character. The value of bandgap $E_g = 0.85$ eV is chosen for the calculations by the AMSET code (the term 'bandgap', used in the AMSET code, means the 'activation energy of the donor/acceptor states') because, in this case, the experimental temperature dependence of electric conductivity $\sigma(T)$ of In_2S_3 is close to the several calculated ones, $\sigma(T)$, for the carrier concentrations N_c in the range of $10^{12} - 10^{15}$ cm^{-3} (Fig. 3)." The real bandgap of In_2S_3 (the gap between valence and conduction bands) is equal to $E_g \approx 2.5$ eV [10 –12].

Several other values related to the electron conductivity of In_2S_3 crystal calculated by AMSET are presented in Table 7. The values corresponding to electron effective mass m^*, calculated for the relatively wide range of the free electron concentrations, are more than three times smaller than the free electron mass m_e.

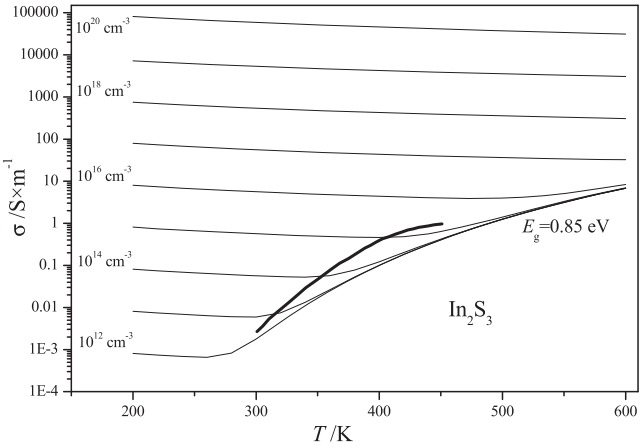

Fig. 3. Temperature dependences of specific electrical conductivity $\sigma(T)$ of In_2S_3 crystal at the space group of symmetry no. 141 calculated by VASP an AMSET codes for different free electron concentrations in the range of $10^{12} - 10^{20}$ cm^{-3} (thin lines) and the corresponding experimental dependence obtained for In_2S_3 thin film (Ref. [34]) deposited at the temperature $T_s = 350$ °C and annealed at the temperature $T_a = 300$ °C (thick line).

Table 7
Electrical conductivity σ, effective electron mass m^*, free electron mobility μ, and free electron scattering time τ for different doping concentrations N_c calculated using AMSET code at the temperature 300 K. Negative signs of N_c correspond to the negative charge of electric carriers (electrons).

N_c /cm^{-3}	$-1{\cdot}10^{13}$	$-1{\cdot}10^{14}$	$-1{\cdot}10^{15}$	$-1{\cdot}10^{16}$	$-1{\cdot}10^{17}$	$-1{\cdot}10^{18}$	$-1{\cdot}10^{19}$
σ /S·cm^{-1}	$6{\cdot}10^{-5}$	$5.63{\cdot}10^{-4}$	$5.63{\cdot}10^{-3}$	$5.61{\cdot}10^{-2}$	0.556	5.41	53.3
m^*/m_e	0.28	0.28	0.29	0.29	0.29	0.29	0.29
μ /cm^2/Vs	35.2	35.2	35.1	35	34.7	33.8	33.2
τ /10^{-15} s	5.71	5.71	5.71	5.70	5.69	5.65	5.45

The free electron relaxation time $\tau \approx 5{\cdot}10^{-15}$ s (Table 7) was obtained by approximating the presence of different free electron scattering mechanisms (acoustic deformation potential scattering, ionized impurity scattering, and polar optical phonon scattering). This relaxation time is close to the typical values of τ for the doped semiconductors. On the other hand, the calculated free electron mobility μ for In_2S_3 (Table 7) is one order of magnitude smaller than the reference one $\mu = 400$ cm^{2}V^{-1}s^{-1} [32] and one order of magnitude larger than the reference value $\mu \approx 5$ cm^{2}V^{-1}s^{-1} [33]. These different values of the free electron mobilities $\mu^{(theor)}$ and $\mu^{(refer)}$ are possible because the conformation of the experimentally used samples of the polycrystalline In_2S_3 films may differ from the single crystal structure of In_2S_3 used for the DFT calculations. Large carrier concentrations, $N_c \sim 10^{18}$ cm^{-3}, and electron mobility, 400 cm^2/(Vs), detected experimentally in In_2S_3 films in Ref. [32] at ambient temperature is caused by the non-stoichiometry of the deposited films (excess of indium in comparison to sulfur).

At liquid helium temperature ($T \approx 5$ K), a new reflection peak arises at the frequency $\omega = 100$ cm^{-1} for the In_2S_3 sample annealed at 300 °C (Fig. 4a). No peaks in this spectral range are observed for the as-grown (20 °C), non-annealed sample (Fig. 4b). The frequency $\omega \approx 100$ cm^{-1} corresponds to the energy $E = 1.24{\cdot}10^{-2}$ eV and the temperature $T = 144$ K. An absence of similar reflection peak at room temperature may be explained by the structure reconstruction of the sample at increasing temperature or by the exhausting of the corresponding electron energy states stimulated by increased temperature. An additional study is needed to reveal the origin of the observed effect, in particular, the reflectance spectra measurements of the sample annealed at 300 °C can be performed in the temperature cycling mode. This peak however indicates presence of the local electron states in the intentionally undoped In_2S_3 with the relatively small binding energy $E = 1.24{\cdot}10^{-2}$ eV.

We have performed the *ab initio* calculations of the dielectric function of In_2S_3 in the range of phonon excitations at the tetragonal symmetry of the crystal (space group no. 141) corresponding to the temperatures of $T < 717$ K [25]. The calculated dielectric functions $\varepsilon_2(\omega)$ of In_2S_3 are presented in Figs. 5 and 6 by the red and blue lines together with the corresponding experimentally obtained ones (black lines). Two different forms of the experimental dependences of $\varepsilon_2(\omega)$ observed in Figs. 5 and 6 correspond to the different post-annealing temperature regions, $T_a \leq 200$ °C, and $T_a \geq 250$ °C. Only one wide maximum of $\varepsilon_2(\omega)$ centered at 220°cm^{-1} – 270°cm^{-1} is observed for the lower annealing temperatures $T_a \leq 200$ °C, whereas for the higher temperatures, $T_a \geq 250$ °C, two clear maxima are present in the spectra. The frequencies of maxima of the experimental dependences $\varepsilon_2(\omega)$ of In_2S_3 films are in a good agreement with the frequencies of the theoretical vibration modes (Figs. 5, 6). The validity of the theoretical dependences $\varepsilon_2(\omega)$, characterized by the high peak magnitudes of $\varepsilon_2^{(VASP)}$ (see the right scales of Figs. 5, 6), has been verified by comparing the theoretical and experimental real parts of dielectric functions $\varepsilon_1(\omega)$ at the frequency $\omega = 0$, $\varepsilon_1(0)$. The phonon (ionic) inputs to the static electric permittivity, $\varepsilon_{stat} - \varepsilon_\infty$, obtained from the experiment (data with RefFIT superscripts in Table 5) and from DFT calculations (data with VASP and CASTEP superscripts in Table 5) are comparable if taking into account the experimental inaccuracies and differences in the calculation features of the corresponding codes.

The relatively wide experimental phonon spectral bands of $\varepsilon_2(\omega)$, corresponding to the large post-annealing temperatures $T_a \geq 250$ °C, as compared to the narrow theoretical ones (Figs. 5, 6) are evidently caused by the large phonon line-widths (scattering rates γ) caused by the structure imperfections of the studied In_2S_3 polycrystalline films in comparison to the corresponding perfect single crystal.

Comparing the effect of substrate temperature T_s and post-annealing temperature T_a on the dielectric function $\varepsilon_2(\omega)$ of In_2S_3 films (Figs. 5, 6) one may claim that the post-annealing temperature T_a influences the dielectric function of the films more clearly than the substrate temperature T_s. However, one has to take into consideration that this result may be not only due to the value of temperature but also the duration of the post annealing process.

The appearance of a single non-structured spectral band of the $\varepsilon_2(\omega)$ for the as-deposited films annealed at the temperatures, $T_a \leq 200$ °C (Figs. 5, 6) is related to the known feature where the amorphous

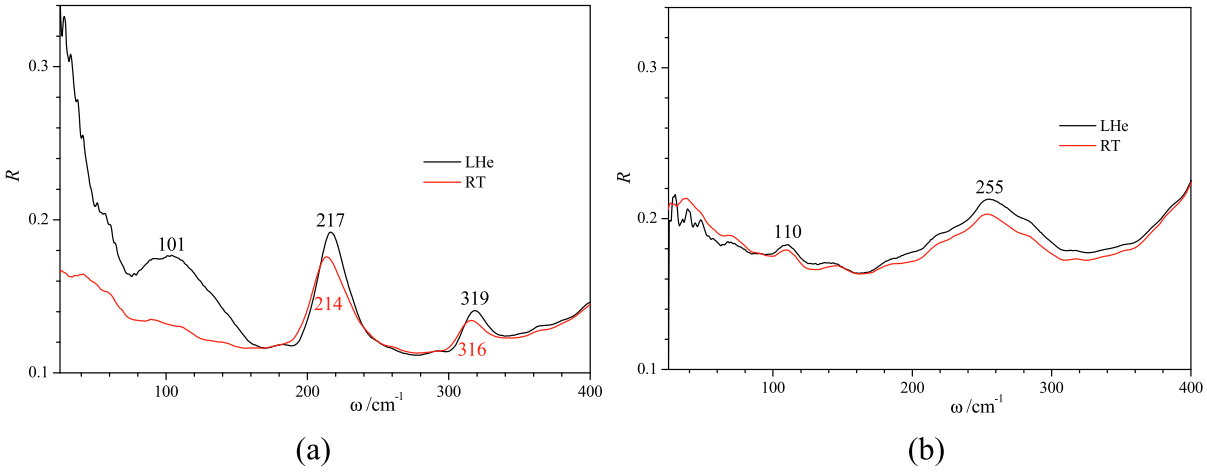

Fig. 4. Reflection spectra of In_2S_3 samples deposited at the temperature 200 °C and measured at 5 K (black lines) and 295 K (red lines) temperatures: (a) annealed at 300 °C and (b) non-annealed.

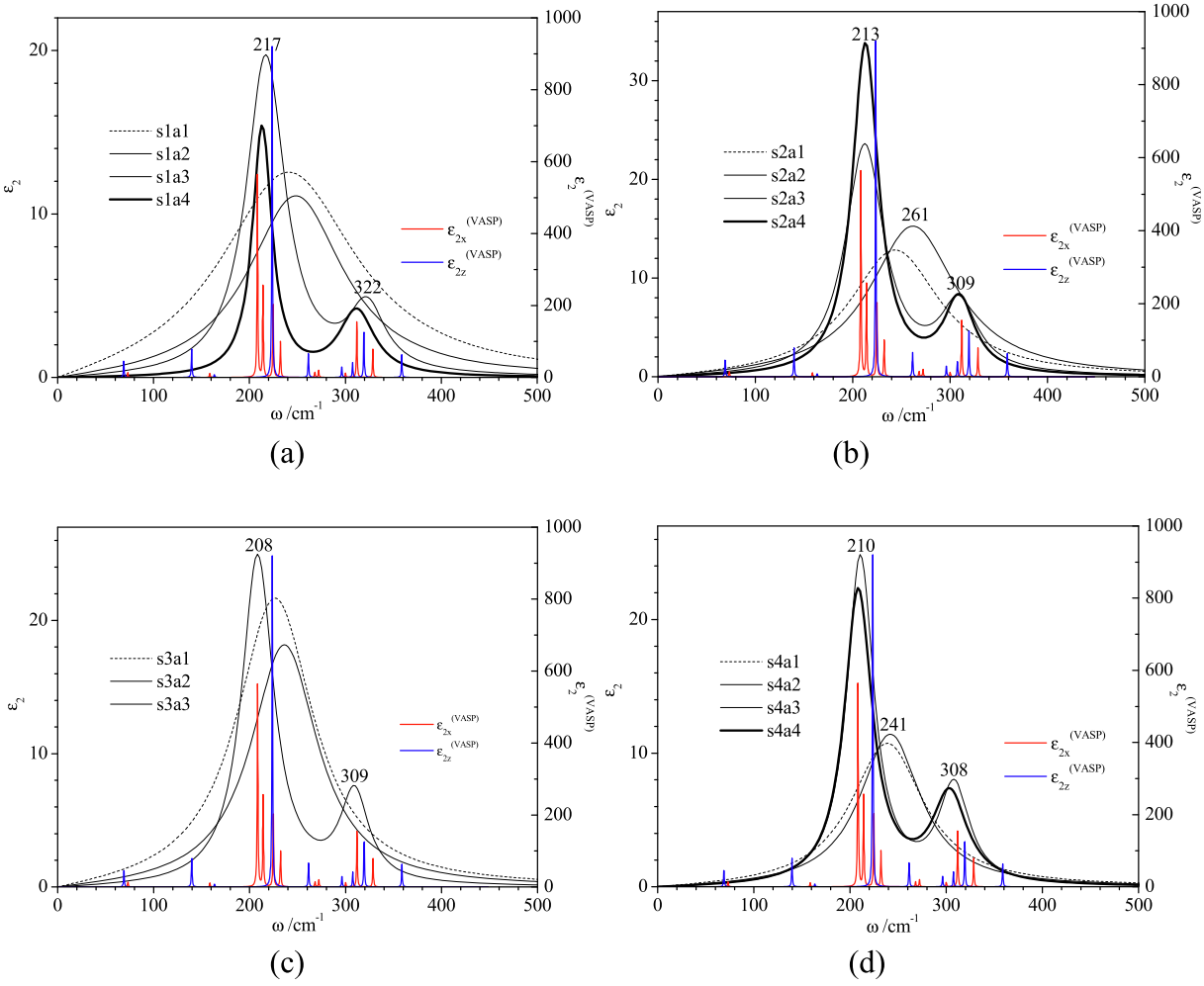

Fig. 5. Experimental (black curves *siaj*) and calculated (red curves $\varepsilon_{2x}^{(VASP)}$, blue curves $\varepsilon_{2z}^{(VASP)}$) imaginary parts of dielectric function $\varepsilon_2(\omega)$ of In_2S_3 films obtained at different substrate (*si*) and post-annealing (*ai*) temperatures, $T_{s1} = 200$ °C, $T_{s2} = 250$ °C, $T_{s3} = 300$ °C, $T_{s4} = 350$ °C, and post-annealing temperatures, $T_{a1} = 20$ °C (a1), $T_{a2} = 200$ °C (a2), $T_{a3} = 250$ °C (a3), and $T_{a4} = 300$ °C (a4) (see Table 2).

structure of the film is caused by its relatively short deposition time. As a result, larger distribution of the interatomic distances in the as-deposited amorphous films occurs in comparison to the polycrystalline ones. This in turn leads to the larger dispersion of the vibration frequencies in the amorphous films in comparison to the polycrystalline ones and justifies the observed non-structured spectral band of the experimental dependence $\varepsilon_2(\omega)$.

We observed no clear changes in the phonon-related spectral bands measured at ambient and liquid helium temperatures. Taking into account that the wide experimental bands are rather formed by the many single ionic vibrations (narrow theoretical phonon peaks in Figs. 5, 6), the mentioned absence of the clear temperature changes of the phonon-related spectral bands indicates small temperature dependence of the phonon–phonon interaction in the studied In_2S_3 thin films.

4. Conclusions

Electron and phonon properties of the intentionally non-doped In_2S_3 thin films are studied on the basis of their FTIR reflection spectra at near normal incidence in the wavenumber range of 30 – 8000 cm^{-1}. For In_2S_3 films studied, no clear reflection spectra features were found in the spectral range 400 – 8000 cm^{-1}, where the excitations of the localized electronic states of In_2S_3 films might in principle take place. The experimental data evidence, that the free electrons concentration in studied In_2S_3 films is less than 10^{15} cm^{-3}. An additional band in the reflection spectra centered at 100 cm^{-1} could be detected at the temperature of about 5 K in the annealed In_2S_3 film, which indicates presence of a localized electronic state of the energy $E = 1.24{\cdot}10^{-2}$ eV. The effective mass of free electrons in In_2S_3 thin films is found to be in the range of $0.5m_e$ – $0.8m_e$, when the theoretical value is equal to $m^* = 0.3m_e$. The free electron concentration N_c in the studied In_2S_3 thin films is estimated to be in the range of $1 \cdot 10^{13}$ – $1{\cdot}10^{15}$ cm^{-3}. The theoretical values of the mobility μ and the relaxation time τ of the free electrons in In_2S_3 crystal of the space group of symmetry no. 141 are found to be $\mu \approx 40$ $cm^2V^{-1}s^{-1}$ and $\tau \approx 5{\cdot}10^{-15}$ s.

By means of XRD it is shown, that the final state of the deposited In_2S_3 thin films depend on the annealing temeprature: anneling of the samples at the temperatures of $T_a \geq 250$ °C leads to crystallization of the material, otherwise amorphous In_2S_3 films are obtained. The amorphous-to-polycrystalline phase transistion also changes the optical properties of the In_2S_3 thin films and the reflection spectra of amorphous and polycrystalline In_2S_3 differ drastically. The structural transition in the films from the amorphous to the polycrystalline state causes the split of one wide vibration band of the imaginary part of the dielectric function $\varepsilon_2(\omega)$, centered at the wavenumber of about 240 cm^{-1} in two well separated narrower bands at about 210 cm^{-1} and 310 cm^{-1}. The intensities of the two latter bands are in approximate relation of 3 to 1, which is in good agreement with the results of the theoretical calculations of the dielectric function, $\varepsilon_2(\omega)$ for In_2S_3 crystal of the tetragonal space group of symmetry no. 141. In view of the absence of the fine

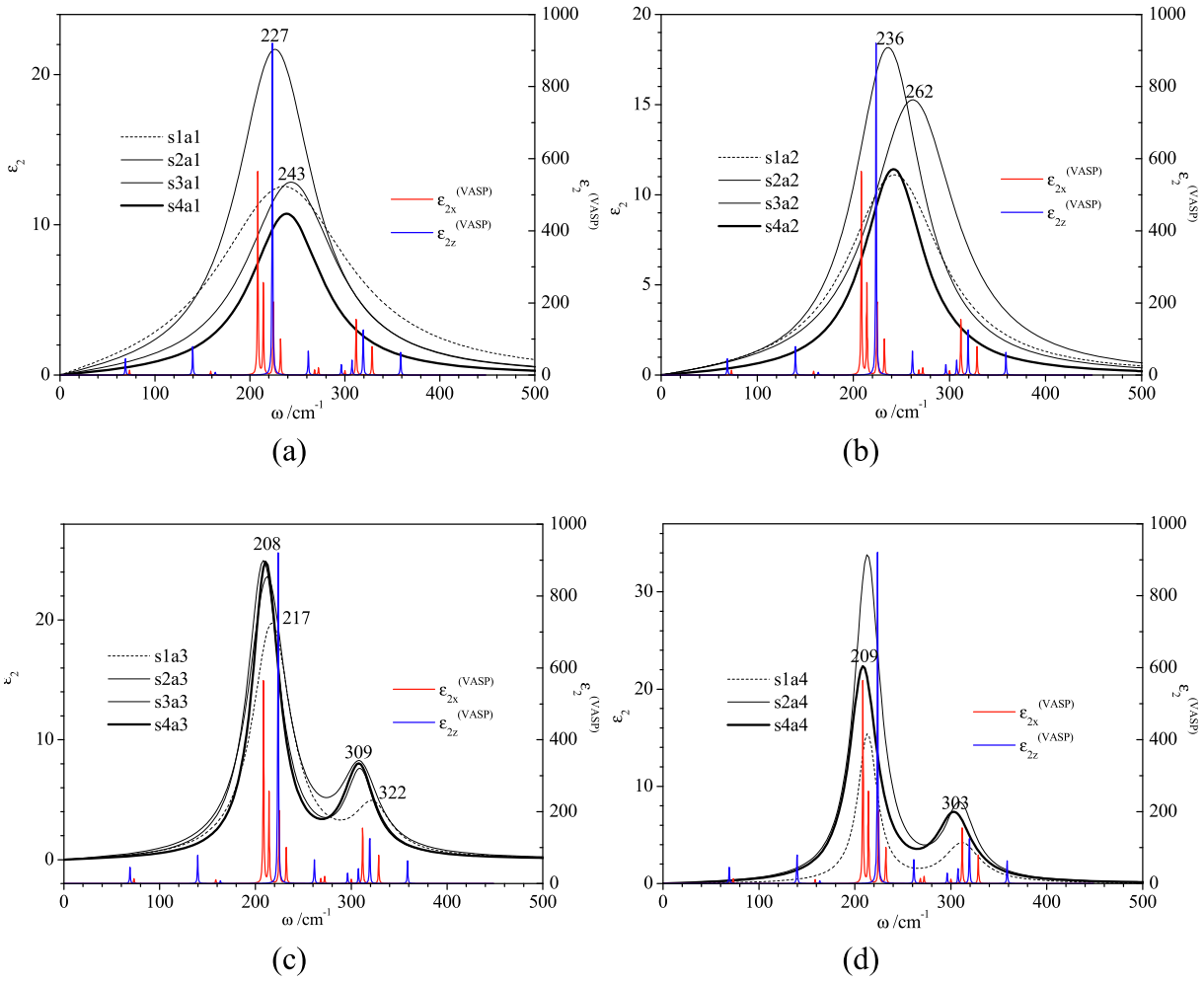

Fig. 6. Experimental (black curves *siaj*) and calculated (red curves $\varepsilon_{2x}^{(VASP)}$, blue curves $\varepsilon_{2z}^{(VASP)}$) imaginary part of dielectric function $\varepsilon_2(\omega)$ of In_2S_3 films obtained at different post-annealing temperatures, (a) $T_a = 20$ °C (a1), (b) $T_a = 200$ °C (a2), (c) $T_a = 250$ °C (a3), and (d) $T_a = 300$ °C (a4), and substrate temperatures, $T_s = 200$ °C (s1), $T_s = 250$ °C, (s2), $T_s = 300$ °C (s3), $T_s = 350$ °C (s4) (see Table 2).

splitting of the separate experimental vibration bands at 210 cm^{-1} and 310 cm^{-1} (such fine splitting takes place in the theoretical dielectric function $\varepsilon_2(\omega)$), it would be interesting to measure the phonon spectrum of the single crystal In_2S_3 and to compare that spectrum with the vibration spectra of the polycrystalline In_2S_3 films.

CRediT authorship contribution statement

Bohdan Andriyevsky: Conceptualization, Methodology, Software, Writing – original draft, Supervision. **Leszek Bychto:** Investigation, Data curation, Software. **Krzysztof Dorywalski:** Investigation, Writing – review & editing. **Ulrich Schade:** Investigation, Visualization. **Ljiljana Puskar:** Investigation, Visualization. **Aleksy Patryn:** Writing – review & editing. **Aneta Hapka:** Software. **Katarzyna Mydłowska:** Investigation, Writing – original draft. **Alexander Veber:** Investigation, Visualization. **Andrii I. Kashuba:** Software. **K.T. Ramakrishna Reddy:** Writing – review & editing.

Declaration of Competing Interest

The authors declare that they have no known competing financial interests or personal relationships that could have appeared to influence the work reported in this paper.

Data availability

Data will be made available on request.

Acknowledgements

Experimental measurements with using the synchrotron radiation of BESSY II operated by the Helmholtz-Zentrum Berlin für Materialien und Energie were performed in the framework of the BESSY proposal 221-10763-ST. Computer calculations were performed at ICM of Warsaw University, Poland (projects No. g86-1023 and g89-1293) and WCSS of the Wrocław University of Technology, Poland (project No. 053).

References

[1] R. Sáez-Araoz, J. Krammer, S. Harndt, T. Koehler, M. Krueger, P. Pistor, A. Jasenek, F. Hergert, M.C. Lux-Steiner, C.-H. Fischer, ILGAR In_2S_3 buffer layers for Cd-free Cu (In, Ga)(S, S_e)2 solar cells with certified efficiencies above 16%, Prog. Photovoltaics Res. Appl. 20 (2012) 855, https://doi.org/10.1002/pip.2268.
[2] Y.J. Hsiao, C.H. Lu, L.W. Ji, T.H. Meen, Y.L. Chen, H.P. Chi, Characterization of photovoltaics with In_2S_3 nanoflakes/*p*-Si heterojunction, Nanoscale Res. Lett. 9 (2014) 32.
[3] H.W. Schock, R. Noufi, CIGS-based solar cells for the next millennium, Prog. Photovoltaics 8 (2000) 151–160.
[4] B. Dimmler, H. Schock, Scaling-up of CIS technology for thin-film solar modules, Prog. Photovoltaics 4 (1996) 425–433.
[5] W. Devaney, W. Chen, J. Stewart, R. Mickelsen, Structure and properties of high efficiency ZnO/CdZnS/CuInGaSe/sub 2/solar cells, IEEE Trans. Electron Devices 37 (1990) 428–433.

[6] M. Nakamura, K. Yamaguchi, Y. Kimoto, Y. Yasaki, T. Kato, H. Sugimoto, Cd-free Cu (In, Ga)(Se, S) 2 thin-film solar cell with record efficiency of 23.35%, IEEE J. Photovoltaics 9 2019 1863-1867. DOI:10.1109/JPHOTOV.2019.2937218.
[7] S. Siebentritt, Alternative buffers for chalcopyrite solar cells, *Sol.* Energy 77 (2004) 767–775, https://doi.org/10.1016/j.solener.2004.06.018.
[8] W. Witte, S. Spiering, D. Hariskos, Substitution of the CdS buffer layer in CIGS thin-film solar cells: status of current research and record cell efficiencies, Vak. Forsch. Prax. 26 (2014) 23–27.
[9] T. Ablekim, J.N. Duenow, X. Zheng, H. Moutinho, J. Moseley, C.L. Perkins, S. W. Johnston, P.O. Keefe, E. Colegrove, D.S. Albin, M.O. Reese, W.K. Metzger, Thin-film solar cells with 19% efficiency by thermal evaporation of CdSe and CdTe, ACS Energy Lett. 5 (3) (2020) 892–896.
[10] S. Rasool, K. Saritha, K.T. Ramakrishna Reddy, K. Raveendranath Reddy, L. Bychto, A. Patryn, M. Maliński, M.S. Tivanov, V.F. Gremenok, Optical properties of thermally evaporated In_2S_3 thin films measured using photoacoustic spectroscopy, Mater. Sci. Semiconductor Processing 72 (2017) 4–8.
[11] S. Rasool, K. Saritha, K.T. Ramakrishna Reddy, L. Bychto, A. Patryn, M. Maliński, M.S. Tivanov, V.F. Gremenok, Optoelectronic properties of In_2S_3 thin films measured using surface photovoltage spectroscopy, Mater. Res. Express 6 (2019), 076417.
[12] S. Rasool, K. Saritha, K.T. Ramakrishna Reddy, M.S. Tivanov, A.V. Trofimova, S. E. Tikoto, L. Bychto, A. Patryn, M. Maliński, V.F. Gremenok, Effect of annealing on the physical properties of thermally evaporated In_2S_3 thin films, Curr. Appl. Phys. 19 (2019) 108–113.
[13] J. Sólyom, Fundamentals of the Physics of Solids, Vol. II, Springer-Verlag, Berlin Heidelberg, Electronic Properties, 2009.
[14] W.G. Spitzer, H.Y. Fan, Determination of optical constants and carrier effective mass of semiconductors, Phys. Rev. 106 (1957) 882–890.
[15] P.Y. Yu, M. Cardona, Fundamentals of Semiconductors, Springer, Heidelberg Dordrecht London New York, 2010.
[16] U. Schade, M. Ortolani, J. Lee, THz experiments with coherent synchrotron radiation from BESSY II, Synchrotron Radiation News 20 (2007) 17–24.
[17] A.B. Kuzmenko, Kramers-Kronig constrained variational analysis of optical data, Rev. Sci. Instrum. 76 (2005), 083108.
[18] G. Kresse, J. Hafner, Ab initio molecular dynamics for liquid metals, Phys. Rev. B 47 (1993) 558–561.
[19] G. Kresse, J. Hafner, Ab initio molecular-dynamics simulation of the liquid-metal-amorphous-semiconductor transition in germanium, Phys. Rev. B 49 (1994) 14251–14269.
[20] G. Kresse, J. Furthmüller, Efficiency of ab-initio total energy calculations for metals and semiconductors using a plane-wave basis set, Comput. Mater. Sci. 6 (1996) 15–50.
[21] G. Kresse, J. Furthmüller, Efficient iterative schemes for ab initio total-energy calculations using a plane-wave basis set, Phys. Rev. B 54 (1996) 11169–11186.
[22] P.E. Blöchl, Projector augmented-wave method, Phys. Rev. B 50 (1994) 17953–17979.
[23] G. Kresse, D. Joubert, From ultrasoft pseudopotentials to the projector augmented-wave method, Phys. Rev. B 59 (1999) 1758–1775.
[24] J.P. Perdew, A. Ruzsinszky, G.I. Csonka, O.A. Vydrov, G.E. Scuseria, L. A. Constantin, X. Zhou, K. Burke, Restoring the density-gradient expansion for exchange in solids and surfaces, Phys. Rev. Lett. 100 (2008), 136406.
[25] P. Pistor, J.M. Merino Alvarez, M. Leon, M. Di Michiel, S. Schorr, R. Klenk, S. Lehmann, Structure reinvestigation of alpha-, beta- and gamma-In_2S_3, Acta. Cryst. B 72 (2016) 410–415, https://doi.org/10.1107/S2052520616007058.
[26] S.J. Clark, M.D. Segall, C.J. Pickard, P.J. Hasnip, M.J. Probert, K. Refson, M. C. Payne, First principles methods using CASTEP, Zeitschrift fuer Kristallographie 220 (2005) 567–570.
[27] A.M. Ganose, J. Park, A. Faghaninia, R. Woods-Robinson, K.A. Persson, A. Jain, Efficient calculation of carrier scattering rates from first principles, Nat. Commun. 12 (2021) 2222.
[28] G. K. H. Madsen, D. J. Singh, BoltzTraP. A code for calculating band-structure dependent quantities. *Comput. Phys. Commun.***175**(2006) 67–71.
[29] C. Julien, H.S. Mavi, Far-IR study of electron-phonon interaction and phase transitions I α-$In_2S_{3-x}Se_x$ ($2.4 \leq x \leq 3.0$), Mater. Sci. Eng. B30 (1995) 27–33.
[30] M. Rubin, Optical properties of soda lime silica glasses, Solar Energy Mater. 12 (1985) 275–288.
[31] M. Dresselhaus, G. Dresselhaus, S.B. Cronin, A. Gomes Souza Filho, Solid State Properties: from Bulk to Nano, Springer-Verlag GmbH, Germany, 2018, p. 317.
[32] M. Hashemi, M. Minbashi, S.M.B. Ghorashi, A. Ghobadi, M.H. Ehsani, M. Heidariramsheh, A. Hajjiah, Electrical and optical characterization of sprayed In_2S_3 thin films as an electron transporting layer in high efficient perovskite solar cells, Solar Energy 215 (2021) 356–366.
[33] R.F. McCarthy, R.D. Schaller, D.J. Gosztola, G.P. Wiederrecht, A.B.F. Martinson, Photoexcited carrier dynamics of In_2S_3 thin films, J. Phys. Chem. Lett. 6 (2015) 2554–2561.
[34] M.S. Tivanov, I.A. Svito, S. Rasool, K. Saritha, K.T. Ramakrishna Reddy, V. F. Gremenok, Effect of heat treatment in sulfur on structural, optical and electrical properties of thermally evaporated In_2S_3 thin films, Solar Energy 222 (2021) 290–297.